

Box for Mask and Mask for Box: weak losses for multi-task partially supervised learning

Hoàng-Ân Lê
hoang-an.le@univ-ubs.fr

IRISA, Université Bretagne Sud,
UMR 6074, 56000 Vannes, France

Paul Berg
paul.berg@irisa.fr

Minh-Tan Pham
minh-tan.pham@irisa.fr

Abstract

Object detection and semantic segmentation are both scene understanding tasks yet they differ in data structure and information level. Object detection requires box coordinates for object instances while semantic segmentation requires pixel-wise class labels. Making use of one task’s information to train the other would be beneficial for multi-task partially supervised learning where each training example is annotated only for a single task, having the potential to expand training sets with different-task datasets. This paper studies various weak losses for partially annotated data in combination with existing supervised losses. We propose Box-for-Mask and Mask-for-Box strategies, and their combination BoMBo, to distil necessary information from one task annotations to train the other. Ablation studies and experimental results on VOC and COCO datasets show favorable results for the proposed idea. Source code and data splits can be found at <https://github.com/lhoangan/multas>.

1 Introduction

Multi-task learning is an active research area of computer vision, in which a shared model is used to optimize multiple targets together from the same input. As such, the model is compelled to learn a shared representation from the task-specific information, thus becoming better generalized and achieving improved performance [36]. Sharing models in the deep learning era also means reducing the number of parameters, or memory footprints, and increasing training and inference speed. As a result, efforts have been made to combine different image-level tasks [30, 35] or those with dense annotations [18, 19, 32, 36, 41].

As the improvement of multi-task learning resulted from the interrelationships obtained by co-training the tasks, the training examples are commonly assumed to be annotated for all the targets. This strong assumption would impede scalability, both in the number of tasks and the number of training examples, as it is expensive to maintain synchronization among the tasks, besides the multiplied annotating efforts. The situation becomes impossible for post hoc tasks requiring synchronized sensor reads, such as depth images.

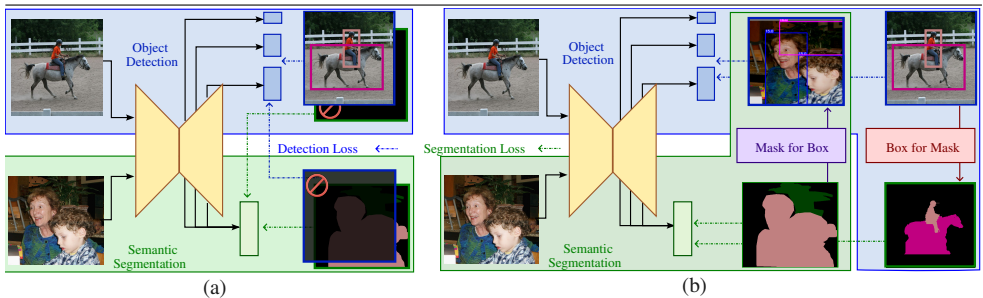


Figure 1: Multi-task partially supervised learning with two tasks, object detection (blue) and semantic segmentation (green). (a) Each image is labeled for a single task, indicated by background colors, thus, can only train the respective head. (b) The proposed Mask-for-Box and Box-for-Mask modules allow training one task head from the other's ground truths.

Multi-task partially supervised learning (MTPSL) introduced by Li *et al.* [10] relaxes the requirements as it allows each training example to associate only with one of the target tasks. Thus, adding a new task to an existing dataset would only involve adding new training examples annotated for the task without having to annotate all the existing images, effectively enlarging the training set. As such, it can also be seen as potentially augmenting the existing task with more examples if the task interrelationship can be learned from such settings.

This exploitation has been demonstrated to improve both tasks' performances by Lê and Pham [11] with a naïve approach where each task is trained only using the respective annotations (Figure 1(a)). Although experiments show favorable results thanks to the improved shared subnet, it is, generally, challenging as the task-specific part of the network cannot be trained with data only annotated for the other task, resulting in diminishing or even negative gain when the target spaces or data domains are too much different.

Inspired by these insights, we hypothesize that providing weak but relevant training signals for one task when the other task's ground truths are available would allow learning better joint representations of both tasks and improve performance. This paper evaluates various weakly-supervised methods of one task given the other's annotations and illustrates the idea with 2 semantic tasks, namely object detection and semantic segmentation as [10]. These tasks, intuitively, are related to one another on the general target of scene understanding yet differ in data structure and information level. Semantic masks identify the object at each pixel yet lack the boundary between instances required for object detection; on the other hand, ground truth bounding boxes enclose the object instance but are short of pixel-wise information. Therefore, extracting the information that improves one task from the other's ground truth would provide more insights into their interrelationship.

Although pseudo-masks, in theory, can be generated from ground truth boxes using unsupervised methods like GrabCut [12], and pseudo-boxes from ground truth masks' circumscribed rectangles, they are insufficient to effectively train a network. To that end, two modules, Box-for-Mask and Mask-for-Box, and their combination BoMBo, are proposed, to refine and make use of one task's annotations and provide targets for training the other (Figure 1(b)). Our contributions, therefore, are:

- We propose a refinement process to extract instance information from semantic masks guided by predicted bounding boxes;

- We evaluate various weak losses for training semantic segmentation from box annotations, and vice versa, with various network architectures;
- We present BoMBo including two modules Box-for-Mask and Mask-for-Box for multi-task partially supervised learning.

2 Related work

2.1 Multi-task partially supervised learning

Multi-task learning has been an interesting topic in the computer vision and machine learning community because of the potential efficiency and improvement over single-task setups. Notable research directions include sharing models [1, 2, 8, 23], balancing task contribution [6, 8, 23], or task relationships [19, 28, 40], of which the dense-prediction tasks such as semantic segmentation, depth, and surface normal are prominent [18, 19, 26].

Multi-task supervised learning [3, 4, 5, 6, 7, 23, 40] is, generally, expensive because of the multiplied efforts to maintain all-task synchronized annotations for the whole datasets. Li *et al.* [19] are the first to coin the term multi-task partially supervised learning and partially annotated data. Different from semi-supervised setups in which limited training data are assumed but still with all task annotations [3, 10], partially annotated data requires each training example to be annotated only for a single task. This paradigm, even with a naïve approach where the model is trained only on the available labels [16], has proven beneficial for improving performance. This paper focuses on scene understanding tasks initiated by Lê and Pham [16], *i.e.* object detection and semantic segmentation, diverging from the dense-prediction task requirement of [19].

2.2 Learning object detection from semantic masks

Training detection heads using semantic segmentation annotations can be considered as a weakly supervised problem in which semantic masks provide the object categories and weak localizing information. The common line of approach (*c.f.* [37]) for weakly-supervised object detection consists of generating pseudo-labels using a duplicated model, called teacher, whose weights are not trained but updated from the main model by exponential moving average (EMA) [17, 26, 39, 40]. The teacher and the student network are, therefore, fed with with same unlabeled inputs but with different augmentation levels.

To the best of our knowledge, no work relies on semantic segmentation ground truths to supervise object detection, intuitively, because pixel-wise semantic masks are more expensive than box annotations. In the context of this paper, semantic masks come from the assumption that a dataset designed for the semantic segmentation task is combined with another for object detection in a multi-task learning framework for the benefit of both tasks.

2.3 Learning semantic segmentation from box annotations

Learning semantic segmentation from box annotations is also a weakly supervised problem. On the one hand, pseudo-masks can be generated from the ground truth bounding boxes with uncertainties using unsupervised methods such as dense CRF [14], GrabCut [31], and M&G+ [11]. On the other hand, the ground truth bounding boxes identify the enclosed objects' categories without delineation, thus can be used to confine predictions and treated as

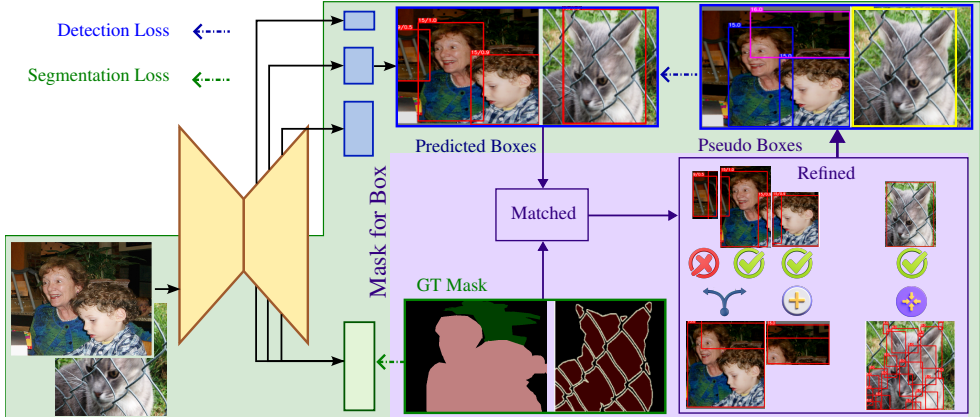


Figure 2: The Mask-for-Box module uses predicted boxes to refine the circumscribed rectangles of the masks’ connected components, by separating \mathcal{Y} multi-instance masks, merging \oplus sub-instance masks, or using as ground truths \oplus . The good \checkmark predicted boxes provide the instance cue while the wrong \times are to be removed.

noisy masks by filling up enclosed areas with class labels. Methods like [33, 34] try to reduce the effect of erroneous gradients from wrong labelling by using filling-rates, as hard constrains [33, 34] or regularization mechanism [35] while box-shape masks are used in attention mechanisms.

3 Method

3.1 Multi-task partially supervised learning

In this paper, we follow the conventional multi-task learning architecture comprising a shared encoder network with backbone and neck subnet for extracting features and decoder heads outputting task-specific predictions. The overview scheme is shown in Figure 1(a). As each training example is annotated for only a single task, not all the losses can be optimized together. Therefore, the network is fed with data annotated for one task after another, and the gradients are computed separately for each head but accumulated for the shared subnet. All parameters are updated once the data for both tasks have been passed through the network. Object detection loss \mathcal{L}_{det} includes the classification Focal Loss [27] and the localization Balanced L1 Loss [29] while the semantic segmentation head uses the regular cross-entropy with softmax loss \mathcal{L}_{seg} . To make up for the lack of corresponding annotations of one task when training the other, the Mask-for-Box losses \mathcal{L}_{M4B} and Box-for-Mask losses \mathcal{L}_{B4M} are proposed to provide pseudo training signals, as shown in Figure 1(b). A detailed architectural scheme can be seen in the supplementary materials. The two task losses are balanced by the parameter λ as follows:

$$\mathcal{L} = (\mathcal{L}_{\text{det}} + \mathcal{L}_{\text{M4B}}) + \lambda (\mathcal{L}_{\text{seg}} + \mathcal{L}_{\text{B4M}}) \quad (1)$$

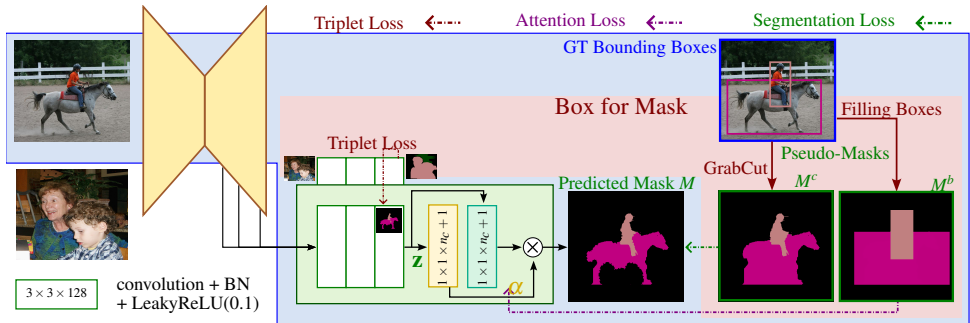


Figure 3: The Box-for-Mask module generates pseudo-masks by filling the ground truth boxes with the same category and an unsupervised-learning method, like GrabCut [31]. The box-shaped pseudo-masks are used to train the attention map α while the other are the predicted masks. The triplet loss constrains the embeddings to follow those with annotations.

3.2 Mask for Box

The Mask-for-Box module is inspired by the observation that the circumscribed rectangles of the connected components in a semantic mask could be considered referenced boxes for training object detection. These boxes correctly identify the object’s category, by definition, but might not the object’s instances, thus introducing noise during training. On the other hand, predicted boxes of a well-trained network have learned to localize object instances, however, with less precision and may fail to recognize the correct object category. The refining idea, therefore, aims to take the best of both worlds by re-localizing the referenced boxes with the guidance of the predicted boxes’ localization information. The process described in Figure 2 shows the Mask-for-Box module applied to two input images. The circumscribed boxes of the connected components in the ground truth masks can be one of the three cases. They may (1) contain multiple object instances, which should be separated (indicated by \textcircled{Y}), (2) cover only a part of an object, which should be merged with other boxes (\textcircled{S}), otherwise (3) they can be directly used for training (\textcircled{P}). The referenced boxes are, first, matched with the predicted boxes following the regular object detection process. The predicted boxes not overlapping with any reference box of the same class are removed (indicated by \textcircled{X}) while those with confidence higher than θ_1 threshold are used for refinement (\textcircled{G}). Reference boxes that cannot be matched to any predicted box are merged before being re-matched. For refinement, as it can be observed that a predicted box should have at least 2 sides touching those of a reference box, a refined box will have the two touching sides from the reference box and the other two from the predicted. Some examples of the refined boxes can be seen in Figure 4 while some failure cases and as well as the pseudo-code can be found in the supplementary materials. Although the same supervised losses can be used for training with refined boxes, only the localization loss is used following the experimental results in Table 1.

3.3 Box for Mask

To train the semantic segmentation head from ground truth bounding boxes, the Box-for-Mask module is proposed. The general scheme is illustrated in Figure 3. Let $\mathcal{C} = \{0, 1, \dots, n_c\}$



Figure 4: Qualitative results of refined boxes with magenta indicate the adding, yellow merging boxes from ground truth masks, and blue for boxes from prediction.

be the set of categories where 0 denotes the background, and $N = w \times h$ the spatial dimension of the input image. Following previous work [15, 33, 34], two types of pseudo-masks are generated from provided ground truth boxes, a box-shaped mask $M^b \in \mathcal{C}^N$ by filling a box-enclosed area with its category, with priority given to the smaller box, and a coarse pseudo mask $M^c \in \mathcal{C}^N$ using an unsupervised method such as GrabCut [35], dense CRF [12], or MCG [11], etc. As it can be observed that a ground truth box provides the upper limit of the object's extent, the coarse mask M^c is filtered by M^b so that $M_i^c = 0, \forall i : M_i^b = 0$, where $M_i^b = 0$ denoting a pixel i in the box-shaped mask not enclosed in any ground truth box, thus surely a background pixel.

Semantic segmentation Loss The final predicted semantic mask M is optimized using the coarse mask M^c following

$$\mathcal{L}_S = -\frac{1}{N} \sum_i^N \sum_{j=0}^{n_c} \mathbb{1}_j(M_i^c) \log \left(\sigma(M_i)_j \right) \quad (2)$$

where $\mathbb{1}_j(x)$ is the indicator function and $\sigma(\mathbf{x})_j = \frac{\exp(x_j)}{\sum_k^{n_c} \exp(x_k)}$, for $j \in \mathcal{C}$ is the softmax function.

Attention Loss Inspired by the previous work where the box-shaped masks are used to train attention masks α , the segmentation head is modified to include an identical and parallel convolution layer (yellow block in Figure 3) to the last layer. Therefore, the attention map $\alpha = [\alpha^j]_{j \in \mathcal{C}} \in \mathbb{R}^{(n_c+1) \times N}$ shares the same dimension with the logit map M^l and $\alpha^j \in \mathbb{R}^N, j \in \mathcal{C}$ is the attention map for class j . The predicted semantic mask M is obtained by modulating the logits as $M = M^l \otimes \alpha$, where \otimes is the Hadamard product. The attention map is optimized using the mean-squared error as shown in Eq. 3.

$$\mathcal{L}_\alpha = \frac{1}{N} \sum_i^N \left\| M_i^b - \alpha_i \right\|^2. \quad (3)$$

Triplet Loss To enforce consistency between predicted representations of un-annotated images, a triplet loss is proposed between the currently predicted ones, called queries, and those with annotations from previous batches, called keys.

Let n_B be the number of ground truth boxes of an image, $\mathcal{B}_k \subset \mathbb{N}^2$ be the *index set* of the pixels within a ground truth box B_k , $k \in \{0 \dots n_B - 1\}$, and $\mathcal{M}_k \subset \mathcal{B}_k$ the *index set* of the pixels having the same class prediction with B_k , or $\text{argmax}(M_i) = c_k, \forall i \in \mathcal{M}_k$. The unit-length mean embedding of the features vectors of the correctly predicted pixels in the bounding box B_k is given by $\bar{\mathbf{z}}_k = \frac{1}{|\mathcal{M}_k|} \sum_{j \in \mathcal{M}_k} \mathbf{z}_j$, where $\|\bar{\mathbf{z}}_k\| = 1$ and \mathbf{z} is the feature vector input to the attention and logit layers (Figure 3).

The triplet loss of a 3-tuple $(\bar{\mathbf{z}}_k, \bar{\mathbf{z}}_k^+, \bar{\mathbf{z}}_k^-)$ is defined as

$$\mathcal{L}_{\text{object}} = \sum_{k \in 0 \dots n_B} \max(0, \gamma + d_{\mathbb{E}}(\bar{\mathbf{z}}_k, \bar{\mathbf{z}}_k^+) - d_{\mathbb{E}}(\bar{\mathbf{z}}_k, \bar{\mathbf{z}}_k^-)), \quad (4)$$

where $\bar{\mathbf{z}}_k^+$ be the embeddings of the same class c_k with \mathbf{z} and $\bar{\mathbf{z}}_k^-$ be the embeddings of different class, $d_{\mathbb{E}}$ is the Euclidean distance and γ is the margin, which is set to 0.1. The Box-for-Mask loss is the sum of all three loses, i.e. $\mathcal{L}_{B4M} = \mathcal{L}_S + \mathcal{L}_\alpha + \mathcal{L}_{\text{object}}$.

4 Experiments

4.1 Setup

Datasets. Most of the experiments are conducted on the Pascal VOC [10] with extra ground truth semantic segmentation from the SBD dataset [11] following the common practices. To simulate the partially-annotated scenario, we divide the training set into two halves, 7,558 images for object detection and 7,656 for semantic segmentation following [16] and report results on the 1,443-image validation set. The COCO dataset [20] is used for the final result report. To simulate data scarcity, one-eighth of the training set (14,655 images) is uniformly sampled for training the detection task and another one-eighth (14,656 images) for semantic segmentation. The results are reported on the provided validation set of 5,000 images.

Implementation. For backbone architectures, the ResNet (-18 and -50) and the Swin-Transformer [27] (-T, -B, -L) families are used. The FPN neck [21] is used with ResNet18 following [16], and PAFPN neck [22] for the rest. The networks are trained for 70 epochs using SGD with a learning rate of $1e-3$. We use the implementation of [16] which includes

Training	\mathcal{L}_{M4B}	ResNet18	ResNet50	SwinT	SwinB
Baseline		50.959	56.286	54.522	59.986
GT Masks	C	49.611	54.843	54.236	58.380
	L	50.168	56.588	55.296	59.473
	L+C	50.617	54.540	54.546	58.567
M4B Refined	C	50.396	55.187	55.625	60.036
	L	52.101	56.486	56.392	61.351
	L+C	48.031	51.787	56.283	60.508

Table 1: Performance of M4B losses, including a localization (L) and/or a classification loss (C), when combining mask-annotated and supervised images (baseline). M4B refinement with only localization loss outperforms using directly GT Masks’ circumscribed rectangles.

ResNet50		Cls \downarrow	Loc \downarrow	Both \downarrow	Dupe \downarrow	Bkg \downarrow	Miss \downarrow	FP \downarrow	FN \downarrow
Baseline		2.66	5.27	0.69	0.24	1.61	6.69	9.09	12.38
M4B Refined	C	2.82	6.05	0.74	0.25	1.42	7.63	9.29	13.46
	L	2.76	5.74	0.66	0.31	1.36	6.48	9.47	12.19
	L+C	2.55	7.28	0.68	0.27	1.64	7.79	11.91	12.92

Table 2: TIDE analysis for 3 configurations (L, C, L+C) of training with M4B Refined boxes on ResNet50. C only does not really improve Cls score but L+C does yet with the cost of Loc. L configuration has the most improvement especially on Miss and FN scores.

an EMA-updated network to collect trained parameters from the one trained with SGD. The EMA network is also used for the unbiased teacher [25] in Table 3 and the B4M triplet loss.

Evaluation and analysis. For object detection, the mAP metric implemented by Detectron2 [38], which averages APs at multiple IOU thresholds in $[0.5, 0.55, \dots, 0.95]$, is used and, for semantic segmentation, the conventional IOU score [12]. For analyzing the error sources, the TIDE [1] framework is used with AP50-detection results, which shows 6 error types, including **Cls**, localizing correctly but not classifying, **Loc**, the other way around, **Both**, localizing and classifying incorrectly, **Dupe**, overlapping with a higher-scoring detection, **Bkg**, detecting background as foreground, **Miss**, all undetected ground truths not already covered, as well as false positive **FP** and false negative **FN**.

4.2 Mask for Box

In this section, we confirm the benefit of M4B loss for object detection. We compare two cases, when the circumscribed rectangles of the ground masks are used directly as referenced boxes for training (GT Masks) and when they are refined using the M4B. The results with classification loss (C) and both localization and classification (L+C) for pseudo targets are also shown for the ablation study. The results are shown in Table 1. It can be seen that using directly the ground truth masks’ circumscribed rectangles would improve over the baseline due to more information being used and using M4B-refined boxes furthers the performance. Surprisingly, involving the classification loss when training with pseudo-targets (C and L+C) results in sub-optimal performance given that the pseudo-boxes’ categories are correct by

		ResNet18	ResNet50	SwinT	SwinB
Baseline	●	50.959	56.286	54.522	59.986
GT Masks	●	50.168	56.588	55.296	59.473
U-Teacher [25]	●	EMA	34.882	43.008	49.726
M4B Refined	●	EMA	52.101	56.486	56.392
U-Teacher [25]	●	pre-trained	51.464	57.408	53.236
M4B Refined	●	pre-trained	53.517	57.721	56.534
					60.956

Table 3: Employing M4B refinement with unbiased teacher knowledge distillation [25]. Using pre-trained networks brings improvement, which can be pushed further by M4B refinement, while directly using EMA predictions as targets produces harmful effects.

		ResNet18	ResNet50	SwinT	SwinB
Baseline	●	65.292	69.065	75.012	79.690
+ \mathcal{L}_S	●	64.740	67.582	73.830	78.510
+ \mathcal{L}_α	●	67.623	71.763	76.269	80.654
+ B2S Affinity [15]	●	66.954	71.562	76.266	80.880
+ Shifting Rate [32]	●	67.325	71.164	76.657	81.264
+ $\mathcal{L}_{\text{object}}$	●	68.545	72.306	76.981	81.236

Table 4: Performance of B4M losses when training box-annotated with supervised images (baseline). Simply applying cross-entropy loss (\mathcal{L}_S) on pseudo-masks (without attention maps) produces negative effects but adding the attention loss (\mathcal{L}_α) provides a boost. The triplet object loss ($\mathcal{L}_{\text{object}}$) is generally more helpful than the other approaches.

definition. The setting with only localization loss (L) consistently attains high performance. The TIDE analysis for ResNet50 in Table 2 shows that although L+C losses reduce CIs error, the pseudo-boxes, generally, do not help improve accuracy (Cls, Loc, Dupe), yet training with pseudo-boxes for localization only is beneficial for FN (Bkg, Miss, FN) errors.

In Table 3, M4B refinement is used with knowledge distillation, in particular, the Unbiased Teacher [25] idea where the predictions, either from the EMA or a pre-trained network, are used as targets to train the current network. Without deviating input augmentation for teacher and student, which over-complicates the training pipeline, the same input images are used for both teacher (EMA/pre-trained) and student (SGD). Using EMA teacher predictions directly results in negative performance due to noises in the target boxes, especially during the first epochs. The pre-trained networks, on the other hand, improve performance as expected with knowledge distillation. M4B-refined runs are generally higher than their counterparts showing the accuracy of the refined boxes.

4.3 Box for Mask

This section validates the design choices for B4M losses. Pseudo-masks generated by Grab-Cut [31] are used for coarse pseudo-masks M^c . Table 4 shows the performance when combining box-annotated with mask-annotated images (baseline) for training semantic segmentation. It can be seen that simply using cross-entropy loss with the pseudo-masks results in

Training	Detection				Segmentation			
	ResNet50	SwinT	SwinB	SwinL	ResNet50	SwinT	SwinB	SwinL
VOC: MTL + BoMBo	55.174 54.885	53.305 54.696	58.267 58.259	59.713 60.687	75.658 74.861	77.795 77.433	81.798 81.205	83.093 83.310
COCO: MTL + BoMBo	17.198 19.087	15.158 16.918	14.914 17.416	19.766 21.935	54.535 58.466	56.280 59.102	63.802 66.420	67.788 68.968

Table 5: BoMBo on VOC and COCO datasets.

negative effects, even with more training data, and half of them are fully annotated. The pseudo-masks, even when confined to only areas within respective ground truth boxes, are noisy and confuse the training process when wrong pixels are used as targets. The attention maps, trained with the box-shaped masks M^b , soften cross-entropy loss’ strong imposition on all pixels, thus helping to take advantage of extra training data. Compared to Shifting Rate [33], which requires fixed statistics pre-computed for each dataset and pseudo-labels, and comparing to Affinity loss [10], the triplet object loss $\mathcal{L}_{\text{object}}$ improves performances.

4.4 Combining Box-for-Mask and Mask-for-Box

In this section, we combine the two previous modules, Box-for-Mask and Mask-for-Box, or BoMBo, in one network for multi-task partially supervised learning. We choose $\lambda = 2$ in Eq. 1 to balance detection and segmentation losses. Table 5 shows the results with and without BoMBo on the VOC and COCO dataset. Although BoMBo outperforms all baselines on COCO, it only excels on both tasks for SwinL on VOC and has mixed results on the other architectures. The results show the benefit of the weak losses in using the extra data available to train one task with the other’s annotations but also suggest an imbalance problem when combining training signals for both tasks.

5 Discussion and Conclusion

The paper investigates various weak losses for training object detection from ground truth semantic masks and vice versa semantic segmentation from box annotations in multi-task partially supervised learning. To that end, the two modules, Box for Mask and Mask for Box and their combination BoMBo, are proposed. The ablation studies show that naïvely extracting shared information to train the other task might result in negative impacts even when supervised data are also being used. The pseudo-boxes, despite having correct categories, can only help when being trained only for localization while pseudo-semantic masks should only constrain the attention-modulated predictions. One limitation of the study is the assumptions of the same data domain and shared class space between the two tasks, which needs to be addressed if partially annotated data are to be used to expand the training set.

Acknowledgments

This work was supported by the SAD 2021 ROMMEO project (ID 21007759) and the ANR AI chair OTTOPIA project (ANR-20-CHIA-0030).

References

- [1] Pablo Arbeláez, Jordi Pont-Tuset, Jon Barron, Ferran Marques, and Jitendra Malik. Multiscale Combinatorial Grouping. In *2014 IEEE Conference on Computer Vision and Pattern Recognition*, pages 328–335, 2014.
- [2] Daniel Bolya, Sean Foley, James Hays, and Judy Hoffman. TIDE: A General Toolbox for Identifying Object Detection Errors. In *ECCV*, 2020.
- [3] Felix J S Bragman, Ryutaro Tanno, Sébastien Ourselin, Daniel C Alexander, and Jorge Cardoso. Stochastic Filter Groups for Multi-Task CNNs: Learning Specialist and Generalist Convolution Kernels. In *Proceedings of the IEEE/CVF International Conference on Computer Vision (ICCV)*, oct 2019.
- [4] David Brüggemann, Menelaos Kanakis, Stamatios Georgoulis, and Luc Van Gool. Automated Search for Resource-Efficient Branched Multi-Task Networks. In *BMVC*, 2020.
- [5] Zhao Chen, Jiquan Ngiam, Yanping Huang, Thang Luong, Henrik Kretzschmar, Yun-ing Chai, and Dragomir Anguelov. Just Pick a Sign: Optimizing Deep Multitask Models with Gradient Sign Dropout. In H Larochelle, M Ranzato, R Hadsell, M F Balcan, and H Lin, editors, *Advances in Neural Information Processing Systems*, volume 33, pages 2039–2050. Curran Associates, Inc., 2020.
- [6] Zhihao Chen, Lei Zhu, Liang Wan, Song Wang, Wei Feng, and Pheng-Ann Heng. A Multi-Task Mean Teacher for Semi-Supervised Shadow Detection. In *Proceedings of the IEEE/CVF Conference on Computer Vision and Pattern Recognition (CVPR)*, jun 2020.
- [7] M Everingham, L Van~Gool, C K I Williams, J Winn, and A Zisserman. The Pascal Visual Object Classes (VOC) Challenge. *ijcv*, 88(2):303–338, jun 2010.
- [8] Yuan Gao, Jiayi Ma, Mingbo Zhao, Wei Liu, and Alan L Yuille. NDDR-CNN: Layerwise Feature Fusing in Multi-Task CNNs by Neural Discriminative Dimensionality Reduction. In *Proceedings of the IEEE/CVF Conference on Computer Vision and Pattern Recognition (CVPR)*, jun 2019.
- [9] Michelle Guo, Albert Haque, De-An Huang, Serena Yeung, and Li Fei-Fei. Dynamic Task Prioritization for Multitask Learning. In *Proceedings of the European Conference on Computer Vision (ECCV)*, sep 2018.
- [10] Bharath Hariharan, Pablo Arbeláez, Lubomir Bourdev, Subhransu Maji, and Jitendra Malik. Semantic contours from inverse detectors. In *2011 International Conference on Computer Vision*, pages 991–998, 2011.
- [11] Abdullah-Al-Zubaer Imran, Chao Huang, Hui Tang, Wei Fan, Yuan Xiao, Dingjun Hao, Zhen Qian, and Demetri Terzopoulos. Partly Supervised Multi-Task Learning. In *2020 19th IEEE International Conference on Machine Learning and Applications (ICMLA)*, pages 769–774, 2020.
- [12] Paul Jaccard. The distribution of the Flora in the Alpine Zone. 1. *New Phytologist*, 1912.

- [13] Alexander Kirillov, Kaiming He, Ross Girshick, Carsten Rother, and Piotr Dollar. Panoptic Segmentation. In *CVPR*, 2019.
- [14] Philipp Krähenbühl and Vladlen Koltun. Efficient inference in fully connected CRFs with Gaussian edge potentials. In *Proceedings of the 24th International Conference on Neural Information Processing Systems*, NIPS'11, pages 109–117, Red Hook, NY, USA, 2011. Curran Associates Inc.
- [15] Viveka Kulharia, Siddhartha Chandra, Amit Agrawal, Philip Torr, and Ambrish Tyagi. Box2Seg: Attention Weighted Loss and Discriminative Feature Learning for Weakly Supervised Segmentation. In *ECCV*, 2020.
- [16] Hoàng-Ân Lê and Minh-Tan Pham. Data exploitation: multi-task learning of object detection and semantic segmentation on partially annotated data. In *British Machine Vision Conference (BMVC)*, 2023.
- [17] Gang Li, Xiang Li, Yujie Wang, Shanshan Zhang, Yichao Wu, and Ding Liang. PseCo: Pseudo Labeling and Consistency Training for Semi-Supervised Object Detection. *arXiv preprint arXiv:2203.16317*, 2022.
- [18] Wei-Hong Li and Hakan Bilen. Knowledge Distillation for Multi-task Learning. In *eccvw*, 2020.
- [19] Wei-Hong Li, Xialei Liu, and Hakan Bilen. Learning Multiple Dense Prediction Tasks from Partially Annotated Data. In *IEEE/CVF International Conference on Computer Vision and Pattern Recognition (CVPR)*, jun 2022.
- [20] Tsung-Yi Lin, Michael Maire, Serge Belongie, James Hays, Pietro Perona, Deva Ramanan, Piotr Dollar, and C Lawrence Zitnick. Microsoft COCO: Common Objects in Context. In David Fleet, Tomas Pajdla, Bernt Schiele, and Tinne Tuytelaars, editors, *eccv*, pages 740–755, Cham, 2014. Springer International Publishing.
- [21] Tsung-Yi Lin, Piotr Dollar, Ross Girshick, Kaiming He, Bharath Hariharan, and Serge Belongie. Feature Pyramid Networks for Object Detection. In *Proceedings of the IEEE Conference on Computer Vision and Pattern Recognition (CVPR)*, jul 2017.
- [22] Tsung-Yi Lin, Priya Goyal, Ross Girshick, Kaiming He, and Piotr Dollar. Focal Loss for Dense Object Detection. In *Proceedings of the IEEE International Conference on Computer Vision (ICCV)*, oct 2017.
- [23] Shikun Liu, Edward Johns, and Andrew J Davison. End-To-End Multi-Task Learning With Attention. In *Proceedings of the IEEE/CVF Conference on Computer Vision and Pattern Recognition (CVPR)*, jun 2019.
- [24] Shu Liu, Lu Qi, Haifang Qin, Jianping Shi, and Jiaya Jia. Path Aggregation Network for Instance Segmentation. In *Proceedings of the IEEE Conference on Computer Vision and Pattern Recognition (CVPR)*, jun 2018.
- [25] Yen-Cheng Liu, Chih-Yao Ma, Zijian He, Chia-Wen Kuo, Kan Chen, Peizhao Zhang, Bichen Wu, Zsolt Kira, and Peter Vajda. Unbiased Teacher for Semi-Supervised Object Detection. In *ICLR*, 2021.

[26] Yen-Cheng Liu, Chih-Yao Ma, and Zsolt Kira. Unbiased Teacher v2: Semi-Supervised Object Detection for Anchor-Free and Anchor-Based Detectors. In *Proceedings of the IEEE/CVF Conference on Computer Vision and Pattern Recognition (CVPR)*, pages 9819–9828, jun 2022.

[27] Ze Liu, Han Hu, Yutong Lin, Zhuliang Yao, Zhenda Xie, Yixuan Wei, Jia Ning, Yue Cao, Zheng Zhang, Li Dong, Furu Wei, and Baining Guo. Swin Transformer V2: Scaling Up Capacity and Resolution. In *International Conference on Computer Vision and Pattern Recognition (CVPR)*, 2022.

[28] Yao Lu, Soren Pirk, Jan Dlabař, Anthony Brohan, Ankita Pasad, Zhao Chen, Vincent Casser, Anelia Angelova, and Ariel Gordon. Taskology: Utilizing Task Relations at Scale. In *Proceedings of the IEEE/CVF Conference on Computer Vision and Pattern Recognition (CVPR)*, pages 8700–8709, jun 2021.

[29] Jiangmiao Pang, Kai Chen, Jianping Shi, Huajun Feng, Wanli Ouyang, and Dahu Lin. Libra R-CNN: Towards Balanced Learning for Object Detection. In *IEEE Conference on Computer Vision and Pattern Recognition*, 2019.

[30] Sylvestre-Alvise Rebuffi, Hakan Bilen, and Andrea Vedaldi. Efficient Parametrization of Multi-Domain Deep Neural Networks. In *Proceedings of the IEEE Conference on Computer Vision and Pattern Recognition (CVPR)*, jun 2018.

[31] Carsten Rother, Vladimir Kolmogorov, and Andrew Blake. GrabCut: Interactive Foreground Extraction Using Iterated Graph Cuts. *ACM Transactions on Graphics (SIGGRAPH)*, 23(3):309–314, aug 2004. ISSN 0730-0301.

[32] Suman Saha, Anton Obukhov, Danda Pani Paudel, Menelaos Kanakis, Yuhua Chen, Stamatis Georgoulis, and Luc Van Gool. Learning To Relate Depth and Semantics for Unsupervised Domain Adaptation. In *Proceedings of the IEEE/CVF Conference on Computer Vision and Pattern Recognition (CVPR)*, pages 8197–8207, jun 2021.

[33] Chunfeng Song, Yan Huang, Wanli Ouyang, and Liang Wang. Box-Driven Class-Wise Region Masking and Filling Rate Guided Loss for Weakly Supervised Semantic Segmentation. In *Proceedings of the IEEE/CVF Conference on Computer Vision and Pattern Recognition (CVPR)*, jun 2019.

[34] Chunfeng Song, Wanli Ouyang, and Zhaoxiang Zhang. Weakly Supervised Semantic Segmentation via Box-Driven Masking and Filling Rate Shifting. *TPAMI*, (12), 2023.

[35] George Stoica, Daniel Bolya, Jakob Bjorner, Taylor Hearn, and Judy Hoffman. ZipIt! Merging Models from Different Tasks without Training. *International Conference on Learning Representations (ICLR)*, 2024.

[36] S Vandenhende, S Georgoulis, W Van Gansbeke, M Proesmans, D Dai, and L Van Gool. Multi-Task Learning for Dense Prediction Tasks: A Survey. *IEEE Transactions on Pattern Analysis and Machine Intelligence*, 44(07):3614–3633, jul 2022. ISSN 1939-3539.

[37] Yanyang Wang, Zhaoxiang Liu, and Shiguo Lian. Semi-supervised Object Detection: A Survey on Recent Research and Progress, 2023.

- [38] Yuxin Wu, Alexander Kirillov, Francisco Massa, Wan-Yen Lo, and Ross Girshick. Detectron2, 2019.
- [39] Mengde Xu, Zheng Zhang, Han Hu, Jianfeng Wang, Lijuan Wang, Fangyun Wei, Xiang Bai, and Zicheng Liu. End-to-End Semi-Supervised Object Detection With Soft Teacher. In *Proceedings of the IEEE/CVF International Conference on Computer Vision (ICCV)*, pages 3060–3069, oct 2021.
- [40] Amir R Zamir, Alexander Sax, Nikhil Cheerla, Rohan Suri, Zhangjie Cao, Jitendra Malik, and Leonidas J Guibas. Robust Learning Through Cross-Task Consistency. In *Proceedings of the IEEE/CVF Conference on Computer Vision and Pattern Recognition (CVPR)*, jun 2020.
- [41] Zhenyu Zhang, Zhen Cui, Chunyan Xu, Zequn Jie, Xiang Li, and Jian Yang. Joint Task-Recursive Learning for Semantic Segmentation and Depth Estimation. In Vittorio Ferrari, Martial Hebert, Cristian Sminchisescu, and Yair Weiss, editors, *Computer Vision – ECCV 2018*, pages 238–255, Cham, 2018. Springer International Publishing.
- [42] Qiang Zhou, Chaohui Yu, Zhibin Wang, Qi Qian, and Hao Li. Instant-Teaching: An End-to-End Semi-Supervised Object Detection Framework. In *Proceedings of the IEEE/CVF Conference on Computer Vision and Pattern Recognition (CVPR)*, pages 4081–4090, jun 2021.

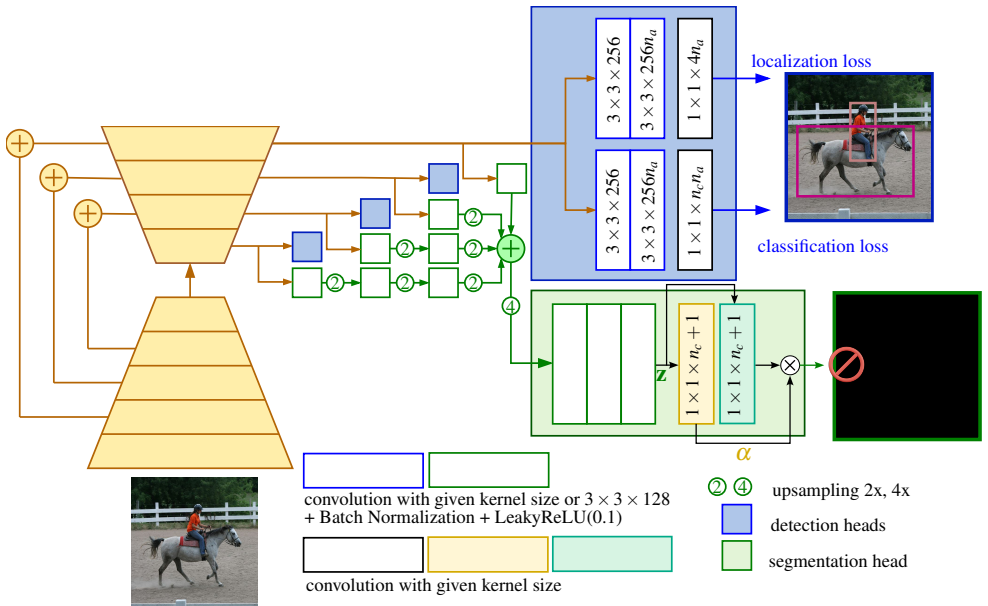


Figure 5: The network architecture being used in the paper, redrawn from [16] with an additional attention module in the segmentation head. The figure is illustrated with a detection-annotated input, thus cannot train the semantic segmentation head.

6 Network architecture

Figure 5 presents the full network, reused from [16], which comprises a backbone and FPN neck as the encoder, a detection head at each FPN level, and a segmentation head using aggregated features from a FPN panoptic [13] subnet. In general, the network architecture is kept unchanged from [16] except an additional attention module in the segmentation head.

7 Mask-for-Box module

Algorithm 1 shows in detail the matching and refining operations for the Mask-for-Box module. The algorithm receives as inputs the ground truth semantic segmentation mask and a list of predicted boxes $\hat{B} = \{(\hat{L}_k, \hat{c}_k)\}_{k=0}^N$ where $N = w \times h$ is spatial dimension of the feature output at each FPN scale, $\hat{L}_k \in \mathbb{R}^4$ is a box localization containing 4 coordinates of a box, and $\hat{c}_k \in \mathbb{R}^{n_C}$ is the vector of confidence scores for each of the n_C category output by a sigmoid function. The `touch` function (L13, 31) makes sure that a predicted box \hat{L}_k touches at least two sides of a reference box L (by comparing to a distance of 10% of the reference box's width and height). The `crop` function (L14, 32) creates a box with the reference box's touching side and the non-touching side of the predicted box. The powerset \mathcal{P} (L21) returns the set of all subsets of \hat{B}^j while the `merge`(p) function creates the smallest box covering all the reference boxes in p . The `unique` function makes sure the same merged box is processed only once. The `leftover` variable contains the referenced boxes to be processed, it first receives all referenced boxes (L10) then has the boxes removed once they are decided

to be either in the splitting (L18) or merging case (L26). The shortlist variable keeps all the predicted boxes matched to the referenced ones which is filtered by the non-maximum impression NMS function (L34). The referenced boxes not recognized for splitting nor merging are added to the output as is.

8 Qualitative results

Figure 6 and 7 illustrate the results of refined boxes from the M4B module. The refined boxes use the best of both worlds, the instance information from the predicted boxes and class information from the ground truth masks to add missing boxes, separate multi-instance boxes, and merge fragmented ones. Some failure cases are shown in Figure 8.

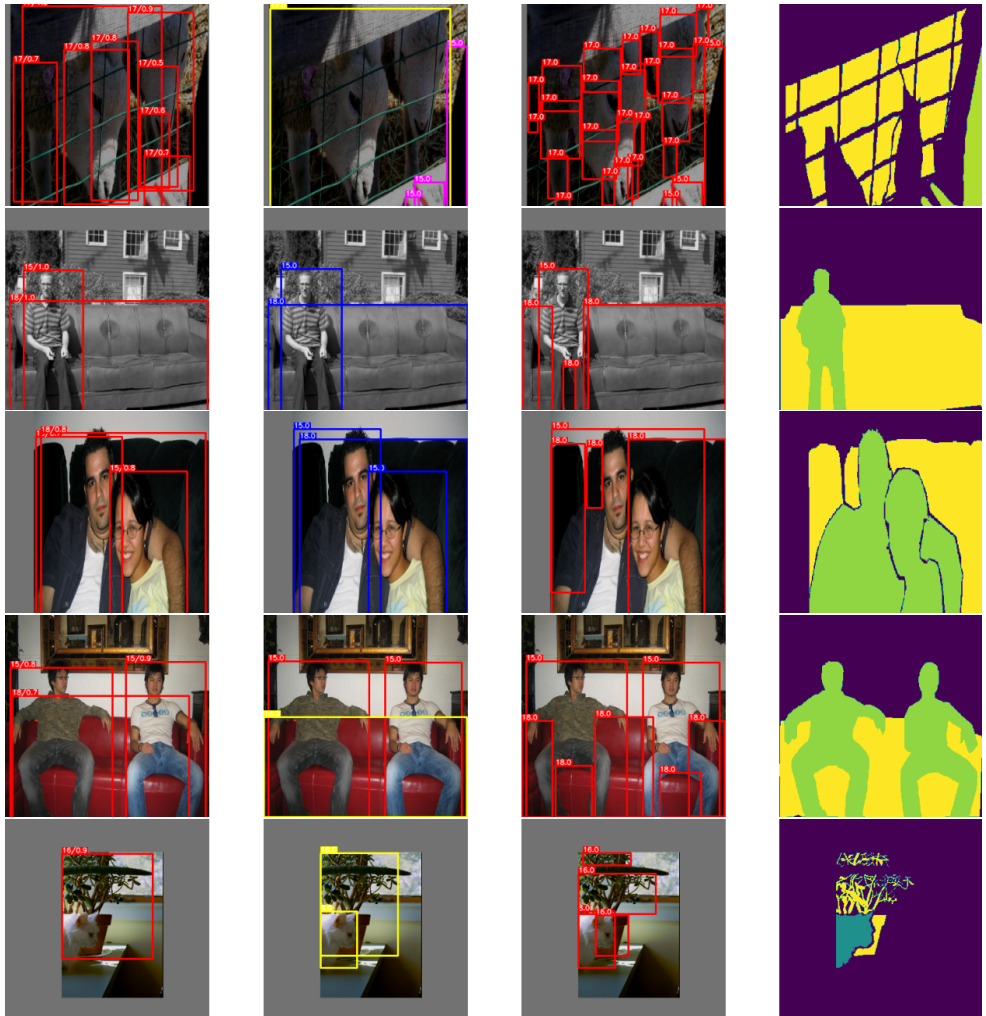


Figure 6: Qualitative results, from left to right: predicted boxes, refined boxes by M4B, boxes from ground truth masks, ground truth masks. The circumscribed boxes of the ground truth follow strictly the connected components, hence can include multiple objects or be fragmented. The refined boxes use the learned information from the predicted box and categories from the masks to obtain better-fitted boxes.

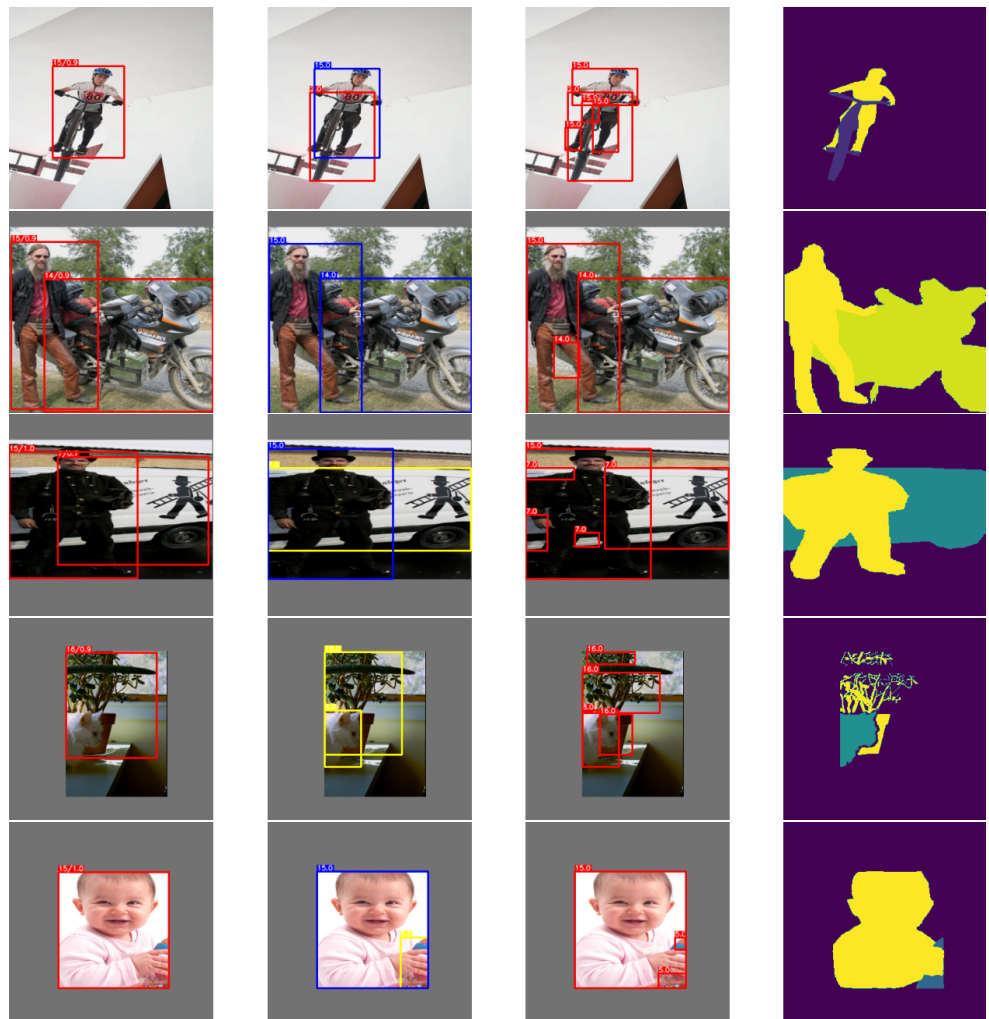


Figure 7: Qualitative results, from left to right: predicted boxes, refined boxes by M4B, boxes from ground truth masks, ground truth masks. The circumscribed boxes of the ground truth follow strictly the connected components, hence can include multiple objects or be fragmented. The refined boxes use the learned information from the predicted box and categories from the masks to obtain better-fitted boxes.

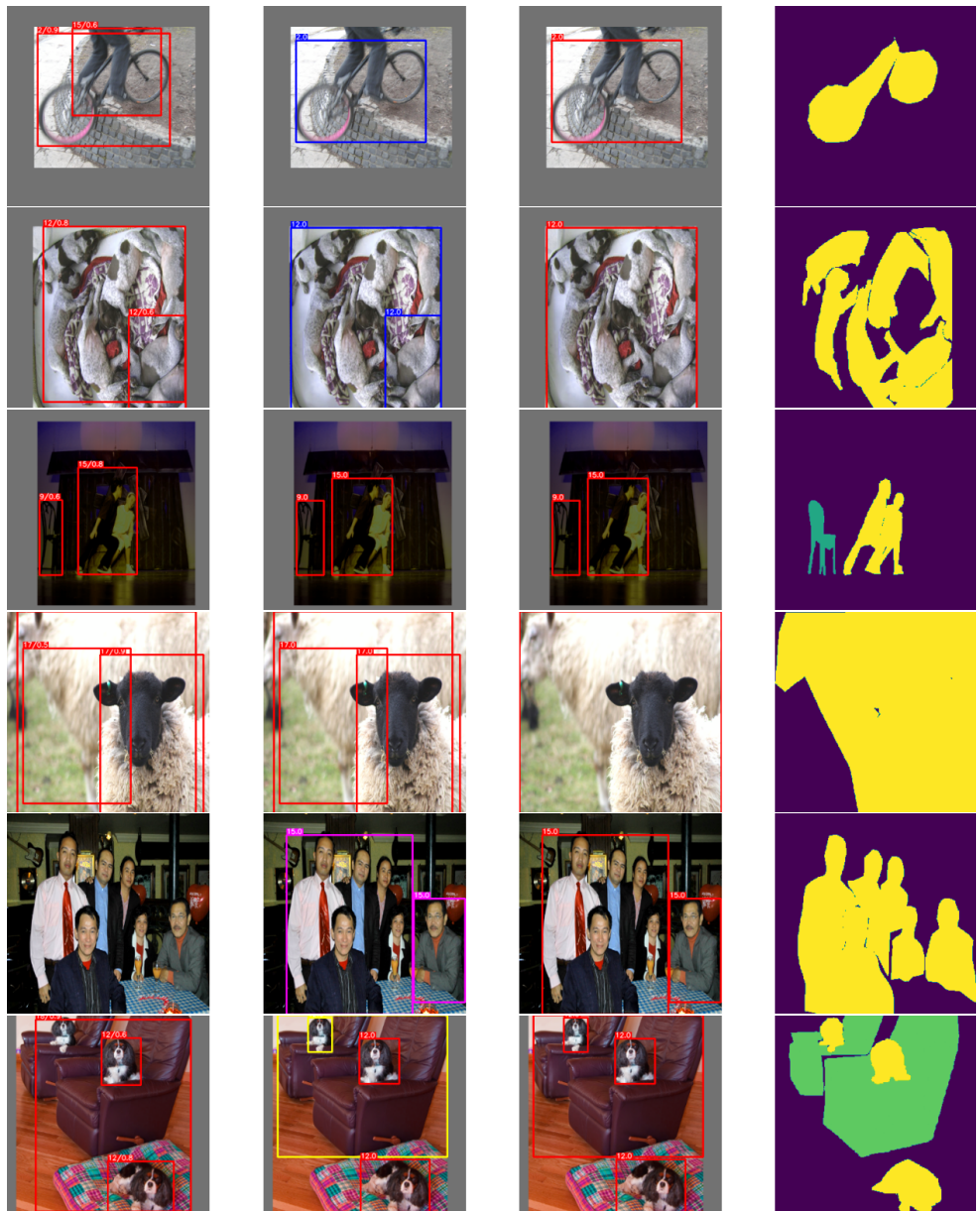


Figure 8: Qualitative results of failure cases, from left to right: predicted boxes, refined boxes by M4B, boxes from ground truth masks, ground truth masks. The refined boxes are incorrect when there is not sufficient information from both sources.